Nanoscale

COMMUNICATION

View Article Online
View Journal | View Issue

Cite this: *Nanoscale*, 2017, **9**, 15286

Received 12th June 2017,
Accepted 11th September 2017

DOI: 10.1039/c7nr04179a

rsc.li/nanoscale

Highly stable $CsPbBr_3$ quantum dots coated with alkyl phosphate for white light-emitting diodes†

Tongtong Xuan, ‡[a] Xianfeng Yang,‡[b] Sunqi Lou,[a,c] Junjian Huang,[a] Yong Liu,[a] Jinbo Yu,[a] Huili Li,[c] Ka-Leung Wong,[d] Chengxin Wang[a] and Jing Wang *[a]

Inorganic halide perovskite quantum dots (QDs) suffer from problems related to poor water stability and poor thermal stability. Here we developed a simple strategy to synthesize alkyl phosphate (TDPA) coated $CsPbBr_3$ QDs by using 1-tetradecylphosphonic acid both as the ligand for the $CsPbBr_3$ QDs and as the precursor for the formation of alkyl phosphate. These QDs not only retain a high photoluminescence quantum yield (PLQY, 68%) and narrow band emission (FHWM ~ 22 nm) but also exhibit high stability against water and heat. The relative PL intensity of the QDs was maintained at 75% or 59% after being dispersed in water for 5 h or heated to 375 K (100 °C), respectively. Finally, white light-emitting diodes (WLEDs) with a high luminous efficiency of 63 lm W^{-1} and a wide color gamut (122% of NTSC) were fabricated by using green-emitting $CsPbBr_3$/TDPA QDs and red-emitting $K_2SiF_6:Mn^{4+}$ phosphors as color converters. The luminous efficiency of the WLEDs remained at 90% after working under a relative humidity (RH) of 60% for 15 h, thereby showing promise for use as backlight devices in LCDs.

Introduction

White light-emitting diodes (WLEDs) have potential applications in displays due to their high luminous efficiency, long lifetimes, low power consumption, fast response, and so on.[1–3] The commercially available WLEDs are based on a blue LED chip with yellow $Y_3Al_{15}O_{12}:Ce^{3+}$ (YAG) phosphors because of their low cost, high luminous efficiency, and simple structure.[4] However, this type of WLED cannot cover sufficient color space due to a lack of green and red components in the emission, which makes its use as backlight devices in liquid-crystal displays (LCDs) difficult. Cadmium chalcogenide quantum dots (QDs) have been widely used in LED displays due to their tunable emission, narrow band emission, high photoluminescence quantum yield (PLQY), and good stability.[5–7] However, the cadmium chalcogenide QDs have some drawbacks such as self-absorption and the need for high reaction temperatures.[8,9]

Lately, all inorganic halide perovskite quantum dots (IPQDs), $CsPbX_3$ (X = Cl, Br, I), have been attracting increasing attention because of their potential applications in light-emitting diodes (LEDs), solar cells, and lasers as a result of their more excellent optical properties, such as a negligible influence of self-absorption, low reaction temperature, high PLQY, wide tunable emission, and narrow band emission, compared to cadmium chalcogenide QDs.[10–16] However, the IPQDs suffer from problems related to poor water stability and poor thermal stability that limit their practical applications.[17–22] Therefore, there is an urgent need for the development of a simple process to synthesize IPQDs that show high stability while preserving a high PLQY and a narrow band emission.[23] To improve the stability of IPQDs, mesoporous silica, polyhedral oligomeric silsesquioxane (POSS), intermolecular C=C bonding, silica matrices, and alumina have been introduced to provide resistance upon exposure to water in moist air.[17,18,21,24–29] Although the obtained composites exhibit improved stability in air, the stability of these IPQDs under extreme conditions, including when dispersed in water or heated to high temperatures, is of greater concern because these composites are not stable enough for practical application.

Coating with an alkyl phosphate layer is a great method that can protect core luminescent materials against water and heat because of its high stability and excellent optical transparency.[30–32] Alkyl phosphate coated on the surface of

[a]*Ministry of Education Key Laboratory of Bioinorganic and Synthetic Chemistry, State Key Laboratory of Optoelectronic Materials and Technologies, School of Chemistry, School of Materials Science and Engineering, Sun Yat-Sen University, Guangzhou, Guangdong 510275, China. E-mail: ceswj@mail.sysu.edu.cn*
[b]*Analytical and Testing Centre, South China University of Technology, Guangzhou, Guangdong 510640, China*
[c]*Engineering Research Center for Nanophotonics & Advanced Instrument, Ministry of Education, School of Physics and Materials Science, East China Normal University, Shanghai 200062, China*
[d]*Department of Chemistry, Hong Kong Baptist University, Kowloon Tong, Hong Kong*
†Electronic supplementary information (ESI) available. See DOI: 10.1039/c7nr04179a
‡These authors contributed equally to this work.

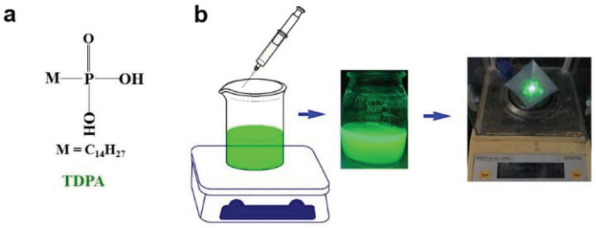

Fig. 1 (a) The molecular formula of TDPA. (b) Schematic illustration of the formation of $CsPbBr_3$/TDPA QDs.

fluoride was found to provide improved water and thermal stability.[33] The formation of alkyl phosphate was based on the esterification of P_2O_5 with alcohols. On the other hand, the alkyl phosphate layer was prepared *via* a self-assembled route in aqueous solutions for passive surfaces and for corrosion protection of metals and metal oxide surfaces.[34–41] However, these approaches cannot be used in the case of IPQDs because the alcohols or water will decompose them before the generation of the alkyl phosphate layers. Thus, the development of a strategy to coat alkyl phosphate over the surface of IPQDs such that they have excellent luminescence properties and high stability is a very worthwhile task to perform. Koh *et al.* reported the synthesis of phosphonic acid stabilized $CsPbX_3$ NCs with improved stability in air *via* a hot-injection route (~150 °C) under the protection of N_2.[42] However, it is hard to apply the hot-injection approach to large-scale synthesis due to complex manipulations and the difficulty in controlling the rate of precursor injection, batch transfer in a short time, and reaction temperature.[6] Moreover, the stability of the QDs dispersed in water and heated to high temperature has not been investigated.

Here, a simple process (Fig. 1) was developed to synthesize $CsPbBr_3$/TDPA QDs under ambient conditions. 1-Tetradecylphosphonic acid was chosen both as the ligand for the $CsPbBr_3$ QDs and as the precursor for the formation of alkyl phosphate. The as-prepared $CsPbBr_3$/TDPA QDs not only retain a high PLQY and a narrow band emission but also exhibit excellent water and thermal stability, which are beneficial to fabricate WLEDs. Therefore, the green-emitting $CsPbBr_3$/TDPA QDs were combined with the red-emitting $K_2SiF_6:Mn^{4+}$ (KSF) phosphors and a blue LED chip to fabricate a WLED that exhibits a wide color gamut and has high luminous efficiency and high stability. These characteristics indicate that the as-prepared QDs are promising green emitters for use in liquid crystal display (LCD) backlight devices.

Results and discussion

To investigate the microstructure of the $CsPbBr_3$/TDPA QDs, the QDs were characterized by transmission electron microscopy (TEM) and X-ray diffraction (XRD). The TEM image of $CsPbBr_3$/TDPA QDs, Fig. 2a, shows that the $CsPbBr_3$ QDs dispersed in alkyl phosphate without evident aggregation. The

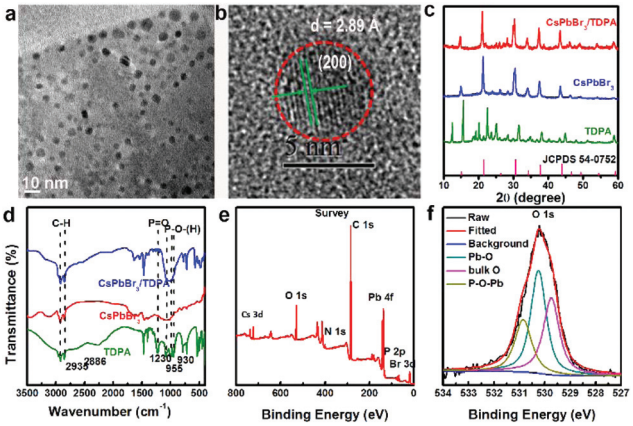

Fig. 2 The (a) TEM and (b) HR-TEM images of $CsPbBr_3$/TDPA QDs. The (c) XRD and (d) FTIR spectra of TDPA, pure $CsPbBr_3$ QDs, and $CsPbBr_3$/TDPA QDs. (e) The XPS spectrum of the QDs. (f) The high-resolution spectra of O 1s.

presence of the alkyl phosphate not only preserves the size of the $CsPbBr_3$ QDs but also effectively separates the $CsPbBr_3$ QDs from each other. The high-resolution TEM (HR-TEM) image (Fig. 2b) of the QDs shows a *d*-spacing of 2.898 Å, which is consistent with the (200) crystal face of cubic phase $CsPbBr_3$.[18] The energy dispersive X-ray spectroscopy (EDS) spectrum (Fig. S2a†), scanning TEM (STEM) EDS-mapping (Fig. S2b†) and EDS line profile spectra (Fig. S3†) of the QDs showed the uniform distributions of P, Cs, Pb, and Br elements. In addition, the XRD patterns (Fig. 2c) of pure $CsPbBr_3$ and the QDs indicate that all their structures belong to the cubic phase (JCPDS no. 54-0752). However, some impure peaks were found in the XRD spectra of the QDs, which were confirmed to be alkyl phosphate on comparison with the XRD spectrum of TDPA.

To verify the process of formation of the $CsPbBr_3$/TDPA QDs, the FTIR spectra (Fig. 2d) of the TDPA and $CsPbBr_3$/TDPA QDs were compared. Before the formation of alkyl phosphate, the FTIR spectrum of TDPA shows the P═O stretching vibration at 1230 cm^{-1} and the P–O–H vibrations at 1000 and 955 cm^{-1}.[34,38,41] However, in the case of the $CsPbBr_3$/TDPA QDs, the vibration of P═O at 1230 cm^{-1} was replaced by a broad peak at 1000–900 cm^{-1} (Pb–O–P),[34,35] which indicates that the P═O bond and the P–O–H bond were gradually broken to produce the Pb–O–P bond, thereby forming alkyl phosphate on the surface of QDs.[33] The absorption bands at 2935 and 2886 cm^{-1} correspond to the vibrations of the C–H groups.[43] Moreover, the X-ray photoelectron spectroscopy (XPS) spectra of the QDs, shown in Fig. 2e, further confirm the presence of P, O, C, Cs, Pb, N, and Br elements on the surface of the QDs. Note that the O 1s spectrum (Fig. 2f) could be fitted to three peaks: P–O–Pb at 530.8 eV, Pb–O at 530.2 eV, and bulk O at 529.7 eV; the assignment of these peaks shows good agreement with the analysis of FTIR spectra (Fig. 2d).

To optimize the optical properties of $CsPbBr_3$/TDPA QDs, the QDs were synthesized with different TDPA concentrations

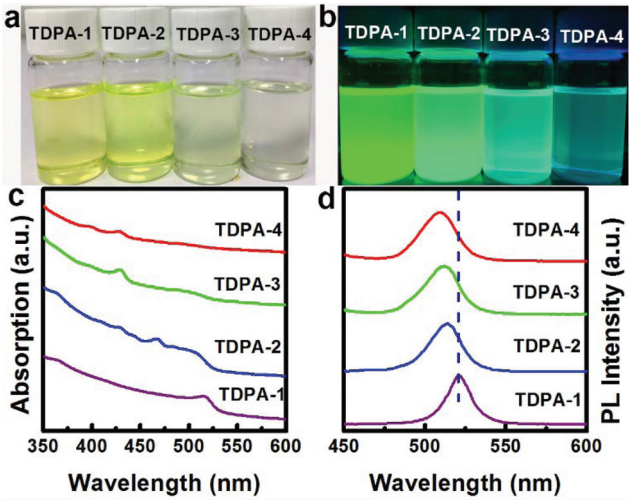

Fig. 3 The images of $CsPbBr_3$/TDPA QDs in (a) daylight and (b) under 365 nm UV light. The (c) UV/vis absorption and (d) PL (d) spectra of $CsPbBr_3$/TDPA QDs with different concentrations of TDPA (TDPA-1: 5 mg mL^{-1}, TDPA-2: 7.5 mg mL^{-1}, TDPA-3: 10 mg mL^{-1}, TDPA-4: 11 mg mL^{-1}).

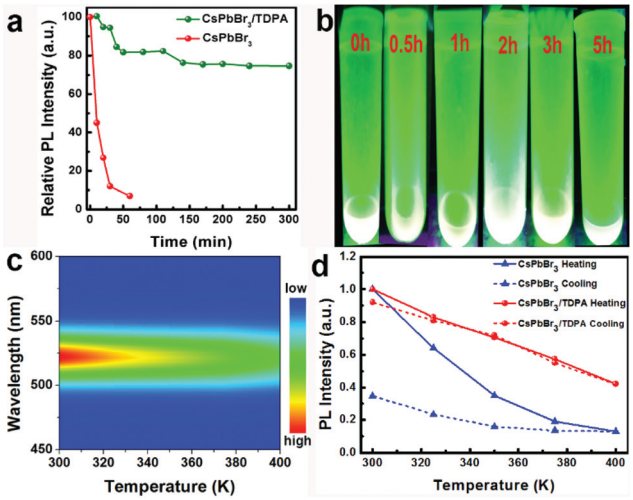

Fig. 4 (a) The relative PL intensity of 0.5 mg mL^{-1} QDs as a function of time in water. (b) Photograph of $CsPbBr_3$/TDPA QDs dispersed in water for different times. (c) Pseudocolor maps of temperature-dependent PL spectra of the $CsPbBr_3$/TDPA QDs (300–400 K). (d) Plots of relative PL intensity of the $CsPbBr_3$/TDPA QDs and pure $CsPbBr_3$ QDs as a function of temperature (300–400 K). The solid line refers to the heating stages and dashed line to the cooling stages.

in the precursor solution. The photographs of the QDs dispersed in solution in daylight and under 365 nm UV light are shown in Fig. 3a and b, respectively. Fig. 3c and d illustrate that their absorption and emission spectra are dependent on the 1-tetradecylphosphonic acid concentration. The absorption and emission spectra exhibit a significant shift to the shorter wavelength with the increase in the concentration of 1-tetradecylphosphonic acid, which indicates the production of smaller $CsPbBr_3$ QDs (Fig. S4†). These are attributed to the increase in the concentration of 1-tetradecylphosphonic acid which causes a decrease in the rate of monomer delivery through the ligand-capping layer. Simultaneously, the highest PLQY of the QDs (68%) was obtained with a narrow band emission (FWHM = 22 nm) when the concentration of 1-tetradecylphosphonic acid increased to 7.5 mg mL^{-1}. Above 7.5 mg mL^{-1}, the PLQY of the QDs started to decrease because the steric hindrance caused by the high concentration of 1-tetradecylphosphonic acid results in a greater number of uncoordinated surface atoms. Note that the PLQY of the $CsPbBr_3$/TDPA powders was preserved at 60%, compared to the low PLQY (<5%) of pure $CsPbBr_3$ powder. This is because the presence of the alkyl phosphate matrix prevents the agglomeration of the $CsPbBr_3$ QDs and fluorescence quenching. In addition, approximately 1.4 g of $CsPbBr_3$/TDPA powder was obtained at one time with a PLQY of 58% and a FWHM of 23 nm.

High stability is the prerequisite for the $CsPbBr_3$/TDPA QDs to be successfully applied to WLED devices. Therefore, the water and thermal stability of the as-prepared QDs was investigated, as shown in Fig. 4. To evaluate the water stability of the $CsPbBr_3$/TDPA QDs and pure $CsPbBr_3$ QDs, 0.5 mg mL^{-1} QDs were dispersed in water with vigorous stirring. The relative PL intensity of the $CsPbBr_3$/TDPA QDs in water remained at 75% of the initial intensity after 5 h, which is much higher than that of pure $CsPbBr_3$ QDs after 1 h (7%). In addition, all the XRD peaks (Fig. S5†) of the $CsPbBr_3$/TDPA QDs immersed in water for different times correspond to cubic $CsPbBr_3$ and alkyl phosphate. These illustrate the excellent water stability of the $CsPbBr_3$/TDPA QDs due to the strong steric hindrance of the alkyl phosphate layers, which reduce the access of water molecules to the surfaces of the $CsPbBr_3$ core QDs. Long-term water stability was also evaluated, as shown in Fig. S6.† The relative PL intensity of the QDs remained at 23% after 210 h. This illustrates that the $CsPbBr_3$/TDPA QDs have high water stability compared to $CsPbBr_3$@POSS, $CsPbBr_3/SiO_2$, $CsPbBr_3$/ZnS, and pure $CsPbBr_3$ QDs.[18,20,21,24,25,44]

To evaluate the thermal stability of $CsPbBr_3$/TDPA QDs, the QDs and pure $CsPbBr_3$ were heated from 300 K to 400 K and cooled back to room temperature while monitoring the PL spectra (Fig. 4c). Remarkably, the relative PL intensity of the QDs preserved approximately 59% of the initial intensity when the temperature increased to 375 K (100 °C) (Fig. 4d), exhibiting much better thermal stability than those of pure $CsPbBr_3$ QDs (19%)[45] and $CsPbBr_3/SiO_2$ composites.[18] In addition, the QDs were heated further up to 400 K that retained the PL intensity of 43%. The QDs still retained 92% of the initial intensity when cooled back to room temperature, which is much higher than that of pure $CsPbBr_3$ QDs (34.8%). The high thermal stability of the QDs may be caused by the increase in the organic content of the alkyl phosphate matrix. Furthermore, the PL intensity of the QDs can be fitted according to eqn (S1),† as shown in Fig. S7.† A binding energy of 279 meV was obtained for the QDs, which is approximately

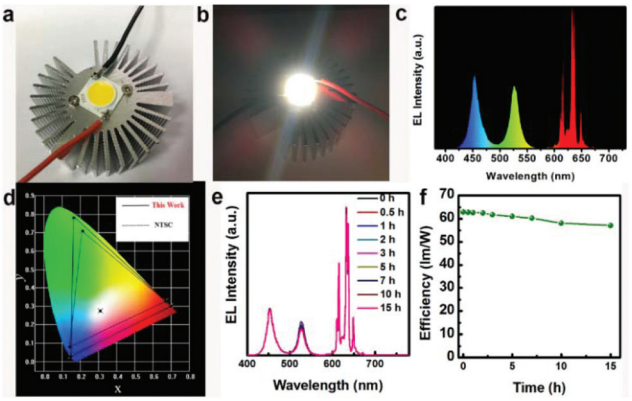

Fig. 5 (a) Photographs of a WLED based on $CsPbBr_3$/TDPA QDs, KSF phosphors and a blue LED chip. (b) The WLED operated at 20 mA. (c) The EL spectrum of the WLED. (d) The color coordinate and the color gamut of the WLED are shown in a CIE 1931 diagram. (e) EL spectra and (f) luminous efficiency of the WLED measured in 60% RH in air for different working times.

eight times higher than that of the bulk $CsPbBr_3$ (approximately 35 meV).[11,46,47] Such a large binding energy implies that the PL emission of the $CsPbBr_3$/TDPA QDs more likely occurs *via* exciton recombination rather than *via* the recombination of free holes and electrons.

The as-prepared green-emitting $CsPbBr_3$/TDPA QDs show high PLQY, narrow band emission, and high stability, making them promising for use as green emitters in display devices. $K_2SiF_6:Mn^{4+}$ (KSF) is a narrow-band red-emitting phosphor with excellent PL properties and higher stability than that of red-emitting IPQDs ($CsPb(Br/I)_3$).[20] In addition, the two phosphors can be well excited at 453 nm without overlap between the PLE spectrum of the red phosphors and the PL spectrum of the green $CsPbBr_3$/TDPA QDs (Fig. S8†). Based on these factors, a WLED (Fig. 5a) was fabricated by encapsulating a mixture of the green-emitting $CsPbBr_3$/TDPA QDs, red-emitting KSF phosphors and silicone resin onto a blue LED chip (λ_{peaks} = 453 nm); this process is similar to the commercial white LED packaging process. As shown in Fig. 5b, the WLED at a driving current of 20 mA generated white emission with a high luminous efficiency of 63 lm W^{-1}, a color rendering index (CRI) of 83, a CIE chromaticity coordinate of (0.31, 0.29), and a color temperature (CCT) of 7072 K without optimizing the structure of the device and these results are a little better than those of the previously reported $CsPb(Br/I)_3/SiO_2$-based WLED (61 lm W^{-1}).[18] The corresponding EL spectrum (Fig. 5c) obviously consists of three emission peaks located at 453, 525, and 631 nm, which belong to the blue LED chip, green QDs and red phosphors, respectively. The CIE color coordinates of WLEDs, blue LEDs, $CsPbBr_3$/TDPA QDs, and KSF phosphors are shown in Fig. 5d, the combination can cover over 122% of the National Television System Committee (NTSC) standard, which shows the wide color gamut of our WLED device. After the WLED worked under a relative humidity of 60% for 5 h, there was no evident change in its EL spectra, indicating a reasonable stability of the device. With a prolonged working time, the intensity of the green band dropped slightly while those of the blue and red bands remained nearly unchanged, which reveals that the $CsPbBr_3$/TDPA QDs are a little more sensitive to blue light than to red KSF phosphors. 15 h later, the luminous efficiency retains 90% (57 lm W^{-1}) of the initial efficiency, which has been compared with the reported WLEDs in Table S1.† These results (Fig. 5e and f) indicate that the PL stability of $CsPbBr_3$/TDPA QDs has been significantly improved and the $CsPbBr_3$/TDPA QDs have potential applications in LCD devices.

Conclusions

In summary, we demonstrated a facile strategy for the synthesis of alkyl phosphate coated $CsPbBr_3$ QDs. The as-prepared QDs were found to not only preserve high PLQY (68%) and narrow band emission (FWHM = 22 nm) but also display high stability against water and heat because of the presence of the alkyl phosphate matrix. Moreover, the green-emitting $CsPbBr_3$/TDPA QDs were combined with the red-emitting KSF phosphors and a blue LED chip to fabricate a WLED. The device exhibited a high luminous efficiency of 63 lm W^{-1} and a wide color gamut (122% of NTSC standard). Moreover, the luminous efficiency of the device degraded a little after working for 15 h. These results imply that the green-emitting $CsPbBr_3$/TDPA QDs have great potential for application in wide color gamut display devices.

Conflicts of interest

There are no conflicts to declare.

Acknowledgements

The authors appreciate the financial support from the National Natural Science Foundation of China (no. 51702373, 51572302 and 51472087), "973" programs (2014CB643801), Teamwork Projects of Guangdong Natural Science Foundation (S2013030012842), the Guangdong Provincial Science & Technology Project (2017A050501008, 2015B090926011 and 2013B090800019), the Natural Science Foundation of Guangdong Province (2014A030313114), New Faculty Start-up funding in the South China University of Technology (SCUT), and the Fundamental Research Funds for the Central Universities from SCUT.

References

1 P. Waltereit, O. Brandt, A. Trampert, H. Grahn, J. Menniger, M. Ramsteiner, M. Reiche and K. Ploog, *Nature*, 2000, **406**, 865–868.

2 E. Jang, S. Jun, H. Jang, J. Lim, B. Kim and Y. Kim, *Adv. Mater.*, 2010, **22**, 3076–3080.
3 S. Nakamura, *Science*, 1998, **281**, 956–961.
4 C. C. Lin and R.-S. Liu, *J. Phys. Chem. Lett.*, 2011, **2**, 1268–1277.
5 H. S. Jang, H. Yang, S. W. Kim, J. Y. Han, S. G. Lee and D. Y. Jeon, *Adv. Mater.*, 2008, **20**, 2696–2702.
6 T.-T. Xuan, J.-Q. Liu, R.-J. Xie, H.-L. Li and Z. Sun, *Chem. Mater.*, 2015, **27**, 1187–1193.
7 S. V. Kershaw, L. Jing, X. Huang, M. Gao and A. L. Rogach, *Mater. Horiz.*, 2017, **4**, 155–205.
8 S. Lou, T. Xuan, C. Yu and H. Li, *Chin. J. Appl. Chem.*, 2016, **33**, 977–993.
9 A. Swarnkar, R. Chulliyil, V. K. Ravi, M. Irfanullah, A. Chowdhury and A. Nag, *Angew. Chem., Int. Ed.*, 2015, **54**, 15424–15428.
10 D. Zhang, Y. Yu, Y. Bekenstein, A. B. Wong, A. P. Alivisatos and P. Yang, *J. Am. Chem. Soc.*, 2016, **138**, 13155–13158.
11 J. Burschka, N. Pellet, S.-J. Moon, R. Humphry-Baker, P. Gao, M. K. Nazeeruddin and M. Grätzel, *Nature*, 2013, **499**, 316–319.
12 W. S. Yang, J. H. Noh, N. J. Jeon, Y. C. Kim, S. Ryu, J. Seo and S. I. Seok, *Science*, 2015, **348**, 1234–1237.
13 N. J. Jeon, J. H. Noh, Y. C. Kim, W. S. Yang, S. Ryu and S. I. Seok, *Nat. Mater.*, 2014, **13**, 897–903.
14 Z.-K. Tan, R. S. Moghaddam, M. L. Lai, P. Docampo, R. Higler, F. Deschler, M. Price, A. Sadhanala, L. M. Pazos and D. Credgington, *Nat. Nanotechnol.*, 2014, **9**, 687–692.
15 X. Zhang, H. Lin, H. Huang, C. Reckmeier, Y. Zhang, W. C. H. Choy and A. L. Rogach, *Nano Lett.*, 2017, **17**, 598–598.
16 H. Huang, L. Polavarapu, J. A. Sichert, A. S. Susha, A. S. Urban and A. L. Rogach, *NPG Asia Mater.*, 2016, **8**, e328.
17 F. Palazon, Q. A. Akkerman, M. Prato and L. Manna, *ACS Nano*, 2016, **10**, 1224–1230.
18 C. Sun, Y. Zhang, C. Ruan, C. Yin, X. Wang, Y. Wang and W. W. Yu, *Adv. Mater.*, 2016, **28**, 10088–10094.
19 Y. Wang, J. He, H. Chen, J. Chen, R. Zhu, P. Ma, A. Towers, Y. Lin, A. J. Gesquiere and S. T. Wu, *Adv. Mater.*, 2016, **28**, 10710–10717.
20 X. Zhang, H.-C. Wang, A.-C. Tang, S.-Y. Lin, H.-C. Tong, C.-Y. Chen, Y.-C. Lee, T.-L. Tsai and R.-S. Liu, *Chem. Mater.*, 2016, **28**, 8493–8497.
21 S. Huang, Z. Li, L. Kong, N. Zhu, A. Shan and L. Li, *J. Am. Chem. Soc.*, 2016, **138**, 5749–5752.
22 X. Li, D. Yu, F. Cao, Y. Gu, Y. Wei, Y. Wu, J. Song and H. Zeng, *Adv. Funct. Mater.*, 2016, **26**, 5903–5912.
23 G. Yang, Q. Fan, B. Chen, Q. Zhou and H. Zhong, *J. Mater. Chem. C*, 2016, **4**, 11387–11391.
24 B. Luo, Y.-C. Pu, S. A. Lindley, Y. Yang, L. Lu, Y. Li, X. Li and J. Z. Zhang, *Angew. Chem., Int. Ed.*, 2016, **55**, 8864–8868.
25 H. Huang, B. Chen, Z. Wang, T. F. Hung, A. S. Susha, H. Zhong and A. L. Rogach, *Chem. Sci.*, 2016, **7**, 5699–5703.
26 H. C. Wang, S. Y. Lin, A. C. Tang, B. P. Singh, H. C. Tong, C. Y. Chen, Y. C. Lee, T. L. Tsai and R. S. Liu, *Angew. Chem., Int. Ed.*, 2016, **55**, 7924–7929.
27 H. Huang, H. Lin, S. V. Kershaw, A. S. Susha, W. C. H. Choy and A. L. Rogach, *J. Phys. Chem. Lett.*, 2016, **7**, 4398–4404.
28 Z. Li, L. Kong, S. Huang and L. Li, *Angew. Chem., Int. Ed.*, 2017, **56**, 8134–8138.
29 S. Lou, T. Xuan, C. Yu, M. Cao, C. Xia, J. Wang and H. Li, *J. Mater. Chem. C*, 2017, **5**, 7431–7435.
30 X. Li, M. Ibrahim Dar, C. Yi, J. Luo, M. Tschumi, S. M. Zakeeruddin, M. K. Nazeeruddin, H. Han and M. Grätzel, *Nat. Chem.*, 2015, **7**, 703–711.
31 R. Hofer, M. Textor and N. Spencer, *Langmuir*, 2001, **17**, 4014–4020.
32 O. Borodin, W. Behl and T. R. Jow, *J. Phys. Chem. C*, 2013, **117**, 8661–8682.
33 H. D. Nguyen, C. C. Lin and R. S. Liu, *Angew. Chem., Int. Ed.*, 2015, **54**, 10862–10866.
34 S. A. Paniagua, A. J. Giordano, O. N. L. Smith, S. Barlow, H. Li, N. R. Armstrong, J. E. Pemberton, J.-L. Brédas, D. Ginger and S. R. Marder, *Chem. Rev.*, 2016, 7117–7158.
35 L. Zeininger, L. Portilla, M. Halik and A. Hirsch, *Chem. – Eur. J.*, 2016, **22**, 13506–13512.
36 F. Reis, H. De Melo and I. Costa, *Electrochim. Acta*, 2006, **51**, 1780–1788.
37 I. L. Liakos, R. C. Newman, E. McAlpine and M. R. Alexander, *Langmuir*, 2007, **23**, 995–999.
38 J. Paul, C. Meltzer, B. r. Braunschweig and W. Peukert, *Langmuir*, 2016, **32**, 8298–8306.
39 I. Maege, E. Jaehne, A. Henke, H.-J. P. Adler, C. Bram, C. Jung and M. Stratmann, *Prog. Org. Coat.*, 1998, **34**, 1–12.
40 C.-M. Ruan, T. Bayer, S. Meth and C. N. Sukenik, *Thin Solid Films*, 2002, **419**, 95–104.
41 J.-e. Qu, C. Geng, H.-r. Wang and D.-j. Nie, *Trans. Nonferrous Met. Soc. China*, 2013, **23**, 3137–3144.
42 W.-k. Koh, S. Park and Y. Ham, *ChemistrySelect*, 2016, **1**, 3479–3482.
43 J. Pan, L. N. Quan, Y. Zhao, W. Peng, B. Murali, S. P. Sarmah, M. Yuan, L. Sinatra, N. M. Alyami, J. Liu, E. Yassitepe, Z. Yang, O. Voznyy, R. Comin, M. N. Hedhili, O. F. Mohammed, Z. H. Lu, D. H. Kim, E. H. Sargent and O. M. Bakr, *Adv. Mater.*, 2016, **28**, 8718–8725.
44 W. Chen, J. Hao, W. Hu, Z. Zang, X. Tang, L. Fang, T. Niu and M. Zhou, *Small*, 2017, **13**, 1604085.
45 F. Zhang, H. Zhong, C. Chen, X.-g. Wu, X. Hu, H. Huang, J. Han, B. Zou and Y. Dong, *ACS Nano*, 2015, **9**, 4533–4542.
46 X. Li, Y. Wu, S. Zhang, B. Cai, Y. Gu, J. Song and H. Zeng, *Adv. Funct. Mater.*, 2016, **26**, 2435–2445.
47 S. Kondo, K. Takahashi, T. Nakanish, T. Saito, H. Asada and H. Nakagawa, *Curr. Appl. Phys.*, 2007, **7**, 1–5.

